

Seismic capacity of brick masonry walls externally bonded GFRP under in-plane loading

Quanfeng Wang^{*1,2}, Zhenling Chai^{2a} and Lingyun Wang^{3b}

¹Xiamen Institute of Technology, Huaqiao University, Xiamen 361021, China

²College of Civil Engineering, Huaqiao University, Xiamen 361021, China

³College of Urban Construction and Safety Engineering, Shanghai Institute of Technology, Shanghai 201418, China

(Received February 20, 2010, Revised January 14, 2014, Accepted April 21, 2014)

Abstract. By carrying out the experiment of eight pieces of brick masonry walls with pilaster strengthened by Glass fiber reinforced polymer (GFRP) and one piece of normal masonry wall with pilaster under low reversed cyclic loading, the failure characteristic of every wall is explained; Seismic performances such as hysteresis, stiffness and its degeneration, deformation, energy consumption and influence of some measures including strengthening means, reinforcement area proportion between GFRP and wall surface, “through-wall” anchor on reinforcement effects are studied. The test results showed that strengthening modes have little influence on stiffness, stiffness degeneration and deformation of the wall, but it is another thing for energy consumption of the wall; The ultimate load, deformation and energy consumption of the walls reinforced by glass fiber sheets was increased remarkably, rigidity and its degeneration was slower; Seismic performance of the wall which considers strengthening means, reinforcement area proportion between GFRP and wall surface, “through-wall” anchor at the same time is better than under the other conditions.

Keywords: cycle tests; glass fiber reinforced polymer (GFRP); reinforcement; brick masonry wall with pilaster; “through-wall” anchor; seismic performance

1. Introduction

Unreinforced masonry (URM) buildings, many of which are of considerable historic and architectural importance, constitute a significant portion of the building stock throughout the world. Due to the fact that many of these buildings have suffered from the accumulated effects of poor construction techniques, material degradation, aging, overloading, foundation settlement, environmental deterioration, enhancement of security, practicability and endurance, old masonry structures often present wide fractures and may be structurally deficient or marginal for current use. In addition to these factors, changing of usage, upgrading of design code, and increasing of the safety requirement have resulted in the need of strengthening or retrofitting for many existing

*Corresponding author, Professor, E-mail: qfwang@hqu.edu.cn

^aEngineering, E-mail: dlzlc@hqu.edu.cn

^bAssociate Professor, E-mail: wangly737@hotmail.com

masonry structures.

Several retrofitting techniques have been adopted for such structures. These include the addition of framing elements to reduce the loads on the walls or surface treatments such as shotcreting or guniting to increase the strength and ductility of the walls. Such retrofits often add significant mass to the structure and are time consuming, costly to carry out, and adversely affect the aesthetics of the upgraded area and in many cases the building as a whole. In the case of seismic retrofitting, the addition of the mass would increase the earthquake-induced inertia forces and may require strengthening of the footing as well. The above disadvantages along with a few other ones related to other traditional strengthening techniques, have recently led researchers to the idea of using fiber-reinforced polymer (FRP) composites that are of the properties of high strength-weight ratio, small thickness and ease of application as strengthening materials by Triantafillou (1998).

The use of new technologies and materials for both restoring and reinforcing masonry structures is technically and economically very interesting. Nowadays, FRP represents a new opportunity to restoring ambit, with considerable development in unreinforced masonry strengthening.

One of the early studies on the use of nonmetallic reinforcement for strengthening of masonry walls was that of Croci *et al.* (1987). A few years later, Sweidan (1991) demonstrated through analytical developments the high effectiveness of a FRP post-tensioning system for prestressing masonry. Schwegler (1994a, b) was the first to propose and study the use of Carbon fiber reinforced polymer (CFRP) as aseismic strengthening elements of masonry structures. The work of Saadatmanesh (1994), Ehsani (1995), Ehsani *et al.* (1997) focused on experimental studies of unreinforced masonry specimens strengthened with epoxy-bonded glass fabrics, leading to the application of the technique to one of the external walls of a one-story commercial building in Glendale, California. Valluzzi *et al.* (2002) performed a series of compressive tests of masonry panels strengthened by FRP laminates. Moghaddam (2004) introduced a new analytical approach for the evaluation of shear strength and cracking pattern of masonry infill panels. Rosenboom *et al.* (2004) assessed the in-plane reversed cyclic performance of post-tensioned clay brick masonry walls constructed with a variety of details. Cecchi *et al.* (2004) proposed a mode for CFRP reinforced masonries by means of homogenization procedures. El-Dakhkhni *et al.* (2004) studied the effect of retrofitting unreinforced concrete masonry-infilled steel frame structures using GFRP laminates. Stratford *et al.* (2004) studied the influence of reinforcement mode: single-sided strengthening and double-sided strengthening on the test results. Hamid *et al.* (2005) studied the in-plane behavior of face shell mortar bedded unreinforced masonry wall assemblages retrofitted with FRP laminates. Static cyclic (ElGawady *et al.* 2004) and dynamic tests (ElGawady *et al.* 2003) on un-reinforced masonry have been done well, the last test shows that the walls' behavior depends on the aspect ratio and the level of the normal force rather than the material properties. Prota *et al.* (2008) investigated in-plane seismic performance of unreinforced masonry walls before and after they are retrofit using FRP materials. An assessment of available design formulas for evaluating both the in-plane performance of unreinforced masonry walls and the contribution of FRP strengthening systems was performed. Lunn *et al.* (2011) evaluated the effectiveness of different externally bonded GFRP for increasing the out-of-plane resistance of infill masonry walls to loading. Parameters investigated in the experiment included aspect ratio, FRP coverage ratio, number of masonry wythes, and type of FRP anchorage. Test results indicated that the type of FRP anchorage had a significant effect on the failure mode. Grande *et al.* (2011) developed a simple procedure for the analysis of the bond behavior of FRP sheets or plates externally applied to

masonry supports for the strengthening or repair of masonry constructions.

All in all, at present, aseismatic researches on masonry structures reinforced with FRP are small and the most studied walls reinforced with fiber reinforced polymer (FRP) just are of the walls with a section of rectangle. In this paper, seismic performance of the brick masonry walls with pilaster by glass fiber reinforced polymer (GFRP) is studied systematically, whose significant research value not only lies in strengthening material (GFRP) but also lies in strengthening object (masonry wall with pilaster).

2. Experimental program

2.1 Specimen design

The objective of this investigation is to determining seismic behavior of brick masonry walls externally bonded GFRP under in-plane loading reversals. Tests and observations have shown that the mechanisms of seismic behavior and failure modes of masonry walls in seismic situation depend mainly on the geometry of the wall. To a great degree, they depend on the ratio of height to width of the wall. The wall should be designed as a squat one. Based on the reviewed test carried out and contrasting between this research and others, the ratio of 0.5 may be justified. It is not practical to test very large walls in the laboratory. These are built as large as possible for the available handling and testing equipment. To simulate even large walls, the specimens are designed as walls with reduced size. For practice related investigation, a carefully selection of the test specimen is required. To be of possible contrast between this research and others, the main bodies of specimens, each having pilaster that has a section of 240 mm×240 mm and the same height of the main body, are of the nominal dimensions of 1500 mm×750 mm×240 mm, see Fig. 1. It is of relevant importance that the boundary restraints and loads acting on the walls, the top RC beam is built for distributing applied vertical and lateral forces evenly. The base of each specimen is anchored rigidly to the bottom RC beam for prevent wall rotation.

Fig. 2 shows the testing arrangement. A combination of vertical compression (representing loads from the building above) and in-plane shear load was applied to each specimen.

The vertical prestress load was applied through two connected hydraulic jacks. This load was distributed across the top of the specimen by a stiff steel reaction beam. The horizontal load (shear

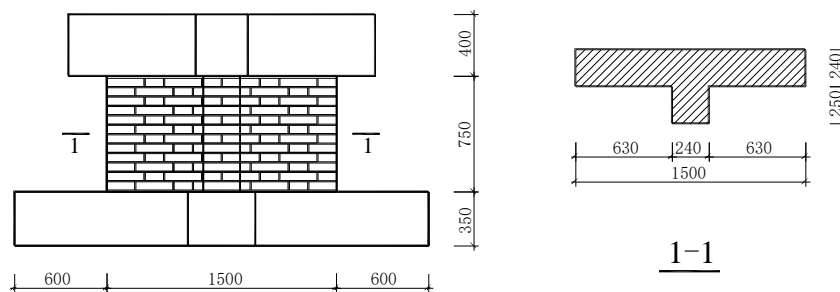


Fig. 1 Dimensions of specimens



Fig. 2 Test apparatus arrangement

Table 1 Details of the masonry specimens

Serial number	Compressive strength of mortar (MPa)	Reinforcement mode	Strip number in single surface (Mode)	Strip width (mm)	Area reinforcement ratio (%)	Volume reinforcement ratio (%)	Anchorage mode
GW1	2.67	----	----	----	----	----	----
GW2	3.55	Horizontal	3 (Horizontal)	100	40.0	0.056	----
GW3	3.38	Mixed	3 (Horizontal) 2 (Gradient)	50 70	40.3	0.057	----
GW4	3.43	Inclined (uniform width)	4 (Secondary) 2 (Primary)	75 75	42.0	0.059	----
GW5	3.15	Gradient (different width)	4 (Secondary) 2 (Primary)	60 90	42.7	0.060	----
GW6	2.32	Inclined (different width)	4 (Secondary) 2 (Primary)	80 120	56.1	0.079	----
GW7	3.11	Inclined (uniform width)	4 (Secondary) 2 (Primary)	80 120	56.1	0.079	Anchorage
GW8	2.68	Inclined (different width)	4 (Secondary) 2 (Primary)	60 90	42.7	0.060	Anchorage
GW9	2.95	Mixed	3 (Horizontal) 2 (Gradient)	70 100	56.7	0.080	Anchorage

load) was applied to the specimen by a horizontal double-acting jack.

Strength of the specimen mainly relates to the following several aspects: the obtained compressive strength of brick is equal to 10.15 MPa; the target compressive strength of mortar is equal to 2.5 MPa and the obtained compressive strength of mortar of every specimen are shown in Table 1; the characteristic of single-direction GFRP in Table 2. In the present experimental work, parameters of the nine pieces of specimens are shown in Table 1. Strengthening schemes of every specimen are shown in Table 1 and in Fig.3. The obtained compressive and shear strength of masonry are 3.56 MPa and 0.22MPa respectively.

Table 2 Material properties of GFRP

Obtained tensile strength (MPa)	Modulus of elasticity (GPa)	Elongation ratio (%)	Nominal thickness (mm)
1507	93.75	1.5	0.169

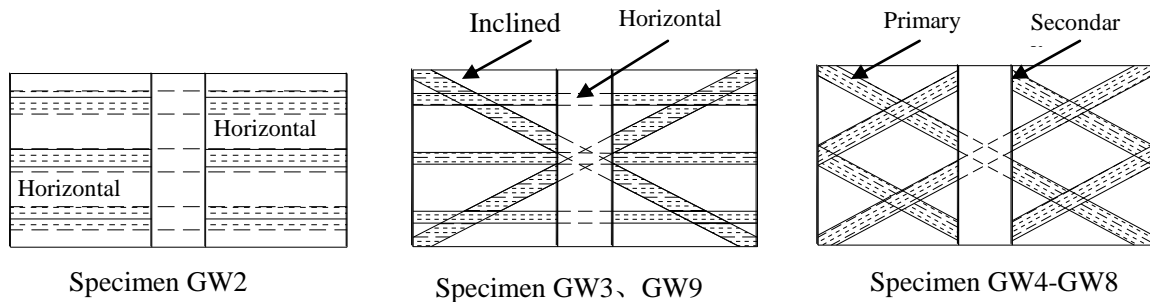


Fig. 3 Reinforcement scheme of specimens

Before applying the GFRP, the specimen was first cleaned from dust and mortar protrusions manually using a wire brush. In this preparation, attention was focused on cleaning the joints and removing excessive mortar and loose particles from the wall surface. A light layer epoxy resin was then applied to the using wall by a hand held paint roller to the wall surfaces. A mixture of the epoxy resin and silica fume was then used to fill the tooled joints and smooth the prepared surface before applying the GFRP. Prior to application on the walls, the dry fabrics were cut to lengths and the epoxy was worked into it with a paint roller. In order to minimize trapped air voids, the roller was run several times on the wet fabrics.

2.2 Loading procedure

Load-displacement control mode was adopted in this study for the load history. Taking the practical loading state of masonry walls into account, a vertical prestress of $N=320$ kN was first applied to the wall, then the horizontal load (P) was done. The peak value of the horizontal load during the first load cycle is 80 kN, from the second load cycle, the horizontal load was increased in increments of 20 kN, at the same time, the pure control displacement (Δ) of the place (O in Fig. 4) where is at the middle of length but the upside of the every specimen should be aware of, when Δ reaches 1 mm, displacement control mode should be substituted for load control mode and the succedent displacement cycles each have a increment of 1 mm. Test was stopped when the horizontal load dropped to 85 percent of the maximal peak value or the specimen breached suddenly.

2.3 Measurement scheme

Vertical load and horizontal load were measured by load transducer and the horizontal deformation was measured by displacement meter, which formed a integrated collection system. Strain gauges were applied to the surface of the GFRP, to measure the strain along the tensile diagonal. The displacement measurement arrangement was shown in Fig. 4.

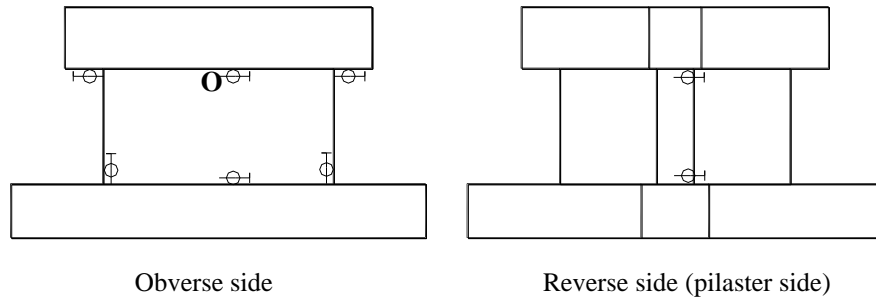


Fig. 4 Displacement measurement arrangement

3. Analysis of experimental results

3.1 Failure of specimens

The first specimen was bare brick masonry wall with pilaster (GW1). The first set of loading was applied to the wall, which was investigated with no signs of concentrated damage. Furthermore, the load-displacement relation was investigated and it confirmed that the wall was still behaving in an elastic manner on condition that the peak value of horizontal load of every cycle is not more than approximately 90 kN. At -188 kN ($P = -188$ kN), the first crack was formed in this wall starting from the bottom corner. With the increasing of the pure control displacement (Δ), this wall began to rock and at 2.6 mm the horizontal load reaches the maximum of all the peak value of every cycle. As the rest of the cycles continued, two dominant cracks occurred at the upper corners which are marked ①② shown in Fig. 5(a). At 4.5 mm, the \times shaped diagonal cracks appeared and the wall was divided into four separate blocks which lead to complete loss of integrity of the wall. The final failure mode of the wall is shown in Fig. 5(a).

The second specimen was the wall whose Reinforcement mode was horizontal (GW2). When the horizontal load P less than 110 kN, no visible phenomena were found. At -190 kN, the first crack is formed at the bottom shown in Fig. 5(b) and propagate toward the vertical centerline of the wall along the mortar bed. At 3.7 mm, the sound of mortar being crushed can be heard and when the pure control displacement reached -6 mm, the uppermost strip ruptured with a loud bang at the middle of it (② shown in Fig. 5(b)), then a dominant crack starting from the place ② formed, the test was stopped. The final failure mode of the wall is shown in Fig. 5(b).

The third specimen was the wall whose Reinforcement was mixed mode which is the combination of horizontal mode and gradient mode (GW3). In order to study the influence of reinforcement mode on the propagation of crack and failure mode, the total reinforcement amount was equal to that of specimen GW2 on condition that the horizontal strips and gradient strips had the same amount. No visible phenomena were found during the preliminary load cycles. At -230 kN, the first crack is formed at the third mortar bed from the bottom shown in Fig. 5(c). At 3.5 mm, one gradient strip ruptured with a loud bang in the vicinity of cross of two strips (① shown in Fig. 5(c)), then At -5.5 mm, the other gradient strip also ruptured in the same way (② shown in Fig. 5(c)). At -6.1 mm, the gradient strip and horizontal strip debonded at the bottom near pilaster

(④ shown in Fig. 5(c)), the debonded length is about 350 mm. The final failure mode of the wall is shown in Fig. 5(c).

The fourth specimen was the wall whose Reinforcement mode was gradient (GW4). The total reinforcement amount was equal to that of specimen GW3 on condition that the width of every strip was same. In the first five cycles, no visible phenomena were found. At 205 kN, the first horizontal crack in the bed joint occurred between the second and third courses from the bottom of the wall, but because of the restriction of the gradient strip, this crack just extended to the outside edge of the strip. As the rest of cycles continued, some visible 45° inclined crack occurred and the wall began to rock with the increase of displacement. When the horizontal load reduced to -236 kN from the maximum of -254 kN, the gradient strip ruptured suddenly at the place of ① shown in Fig. 5(d) and then in the subsequent cycle, at 202 kN, the other principle strip also ruptured at the place of ② shown in Fig. 5(d). The final failure mode of the wall is shown in Fig. 5(d).

In order to research influence of the width of strip on the test results when the reinforcement amount was equal, the fifth specimen was the same as specimen GW4 except that the width of every strip is not equal. During the preliminary several load cycles, the phenomena of the specimen were similar to specimen GW4, but from the first displacement stage, the propagation of 45° inclined cracks were obviously slower than horizontal cracks that occurred between the second and the third courses from bottom, which was dissimilar to specimen GW4. With the increase of the displacement the cracks in the head faces were also formed and severe corner crushing occurred with parts of the wall spalling out at the bottom. At -4.2 mm, one gradient strip ruptured with a loud bang in the vicinity of cross of two strips (① shown in Fig. 5(e)), then At 6.1 mm, the other gradient strip also ruptured in the same way (② shown in Fig. 5(e)). Up to now, the two horizontal cracks that were formed originally at the two bottom corners were jointed. When the pure displacement reached 7.6 mm, then the inclined crack (③ and ④ shown in Fig. 5(e)) also formed, which was the sign of the end of the test. The final failure mode of the wall is shown in Fig. 5(e).

With view to studying influence of the reinforcement amount on the test results when the reinforcement mode was same, the sixth specimen was the same as specimen GW5 except that the reinforcement amount of this specimen was larger than that of GW5. At 217 kN, a first vertical crack initiated at the place of ① shown in Fig. 5(f), then at -3.6 mm, cracking began at the edge of primary strip (② shown in Fig. 5(f)) and at edge of secondary strip (③ shown in Fig. 5(f)). At 3.9 mm, a delamination crack was formed (④ shown in Fig. 5(f)), but the strip wasn't completely separated from the surface of the wall. At 5.6 mm, the strip is debonded from the surface of the wall, the debonded length is about 20 mm. When the pure displacement increased to 5.6 mm, a phenomenon that some close reinforcement region was hollow (can be defined as "hollow phenomenon" was found (for example, the region of ⑤ and ⑥ shown in Fig. 5(f)). With the increase of the pure displacement, the hollow region became larger than ever and the spread of cracks across the masonry was accompanied by local de-bonding of the GFRP from the masonry, so that a band of debonded GFRP formed along a band roughly parallel to the cracks. At 187 kN, the GFRP on the top is debonded from the masonry suddenly, the test was stopped. The final failure mode of the wall is shown in Fig. 5(f).

Specimen GW7 was similar to GW6 except that "through-wall" anchors which were made by narrow strips were used to reduce or avoid the debonding and hollow regions. At 205 kN, cracking initiated at the bottom and then propagated to the edge of pilaster. With the increase of the pure displacement, hollow regions also occurred, but due to the existence of "through-wall" anchors,

the area and number of the hollow regions were less than that of GW6. At -6.0mm, the gradient strip on the top surface of pilaster is debonded with vibrancy ringing, and at 7.9 mm, one principle strip ruptured suddenly, which indicated end of this test. The final failure mode of the wall is shown in Fig. 5(g).

Specimen GW8 was similar to GW5 except that “through-wall” anchors which the anchor amount was equal to GW7 were used. At -198 kN, a horizontal crack occurred at the bottom. Hollow regions can be found and sounds thought to be masonry blocks splitting were heard at -3.8 mm. As the rest of the 8.6 mm cycle continued the wall suffered cracking in the form of inclined starting from the middle of the heading course to bottom corner (③ and ⑤ shown in Fig. 5(h)). The final failure mode of the wall is shown in Fig. 5(h).

Specimen GW9 was similar to GW3 except for the two aspects of reinforcement amount and anchorage measure. For the purpose of comprehensive contrast, the reinforcement amount was similar to GW6 and GW7 and anchorage measure and anchor were same as GW7 and GW8. In the first five cycles, no visible phenomena were found. a horizontal crack was found at the bottom at -198 kN, then small regions of local debonding initially formed near the displacement application point (at -4.5 mm) and the hollow phenomena (① and ③ shown in Fig. 5(i)) occurred which is similar to Specimen GW8. When the pure displacement reached 9.3 mm, a vertical crack in the pilaster starting from the top propagated to the bottom. At -11.2 mm, the gradient strip and horizontal strip debonded from the surface of the wall at the bottom near pilaster with vibrancy ringing (⑤ shown in Fig. 5(i)). At last, the pure displacement reached 22 mm which was much larger than that of the other specimens. The final failure mode of the wall is shown in Fig. 5(i).

3.2 Load-deformation response

The load-displacement relation curve of a structure or its component is called hysteresis curve. The hysteresis curve of masonry wall, the embodiment of deformation record and capacity of coming back to the original state after the load is removed, can be used to describe comprehensively elastic, ductile properties and energy consumption. Hysteresis loop curve is of

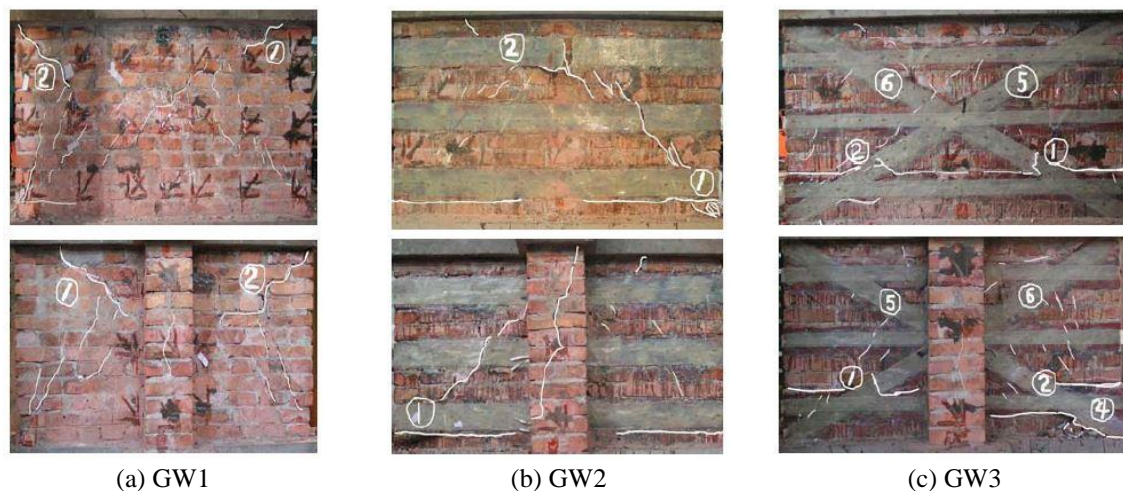


Fig. 5 Failure modes of specimens



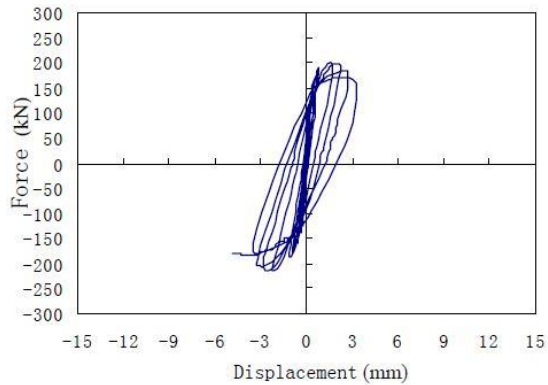
Fig. 5 Continued

four elementary shapes: shuttle shape, arch shape, reverse *S* shape and *Z* shape. For most structures, the shape of hysteresis loop curve often begins with shuttle shape and then develops to arch shape, reverse *S* shape and *Z* shape finally by Li (2004). The hysteresis curve of every specimen was shown in Fig. 6.

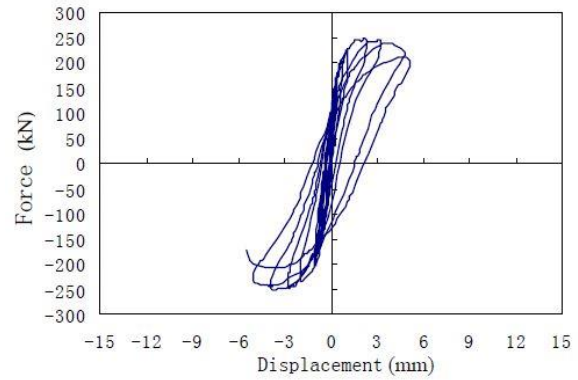
It can be seen from the Fig. 6 that all the hysteresis loop curve of every specimen was of arch shape except for that of specimen GW2 which was the only specimen reinforced only by horizontal strips. As far as specimen GW2 concerned, the horizontal crack at bottom occurred earlier and propagated faster than other specimens, therefore horizontal slide was much larger than that of the others, so the hysteresis curve shape of GW2 was of reverse *S* shape (as shown in Fig. 6(b)) which was different from the others. For specimen GW4, because of the change of loading sequence which was attributed to the testing apparatus, the last hysteresis loop (as shown in Fig. 6(d)) can't be used to make analysis. It was also obvious that the area of hysteresis loop of specimen GW3 and GW9 that was strengthened by horizontal and gradient strips at one time was

much larger than that of other specimens, from which a conclusion could be drawn that specimen reinforced by mixed mode was superior to the other two modes in energy dissipation.

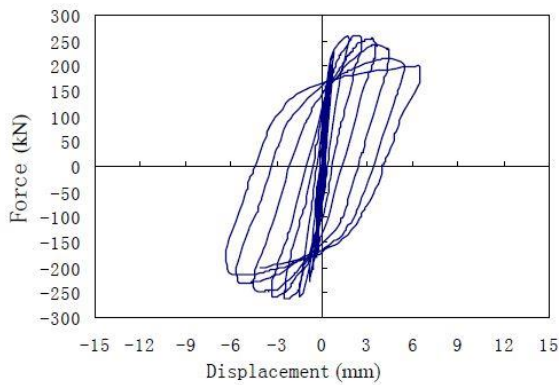
3.3 Envelope response



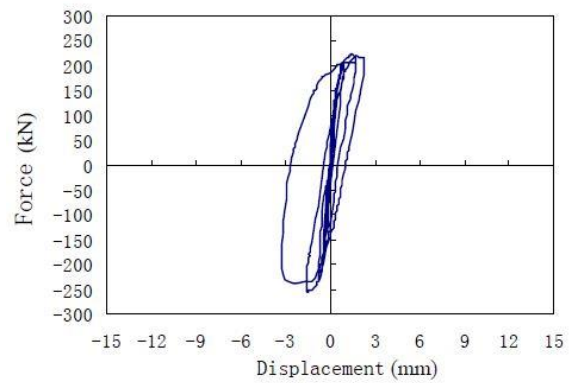
(a) Hysteresis curve of GW1



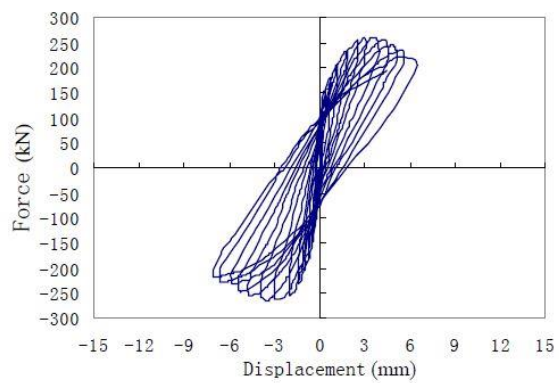
(b) Hysteresis curve of GW2



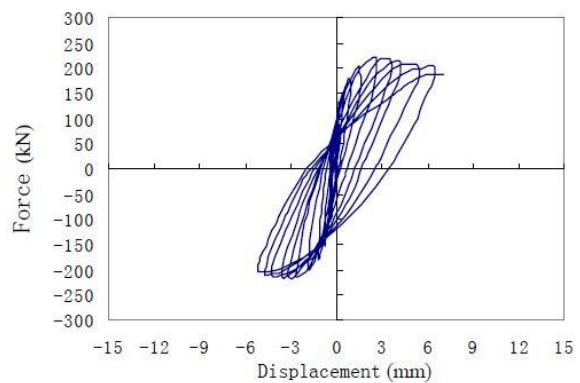
(c) Hysteresis curve of GW3



(d) Hysteresis curve of GW4

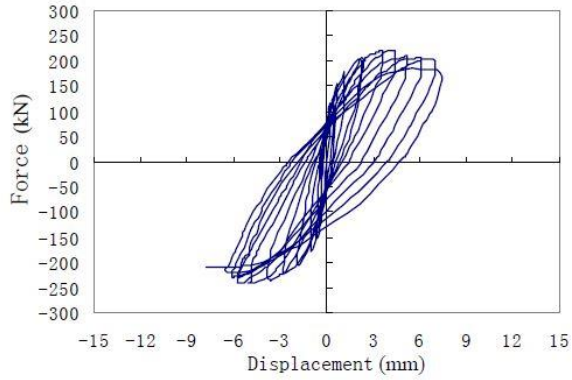


(e) Hysteresis curve of GW5

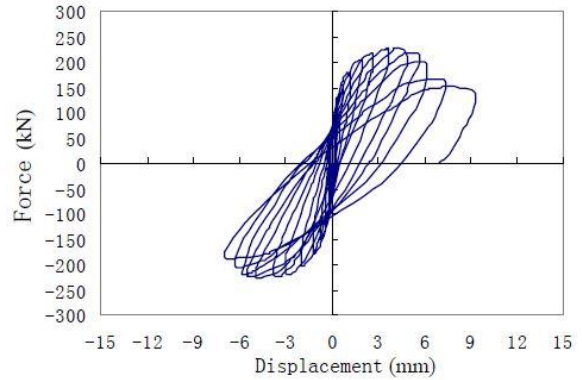


(f) Hysteresis curve of GW6

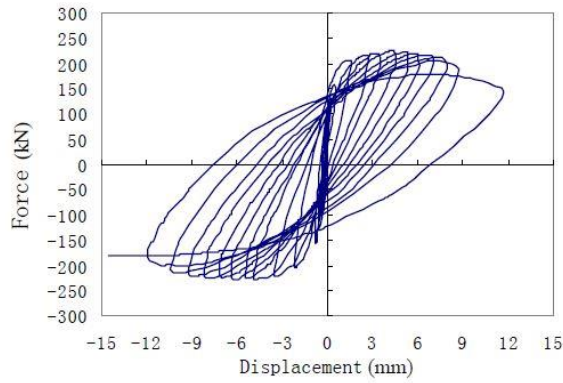
Fig. 6 Load-displacement relation



(g) Hysteresis curve of GW7



(h) Hysteresis curve of GW8



(i) Hysteresis curve of GW9

Fig. 6 Continued

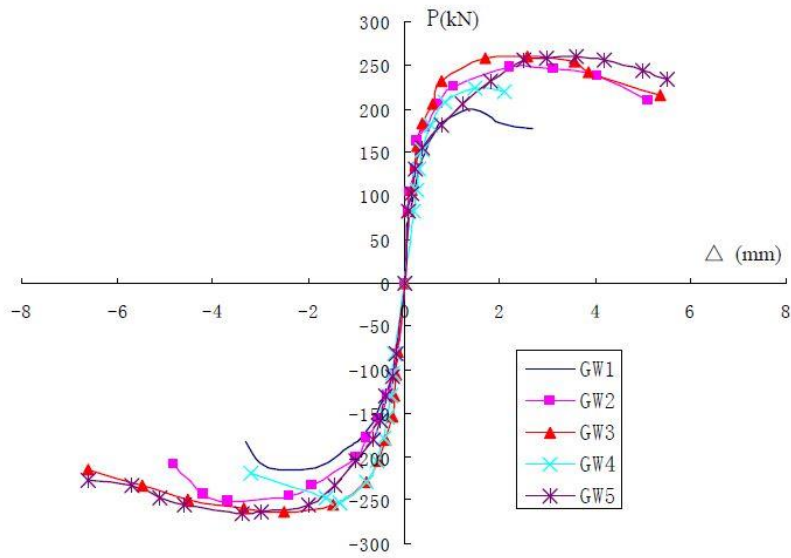


Fig. 7 Skeleton curves of lateral load versus deformation

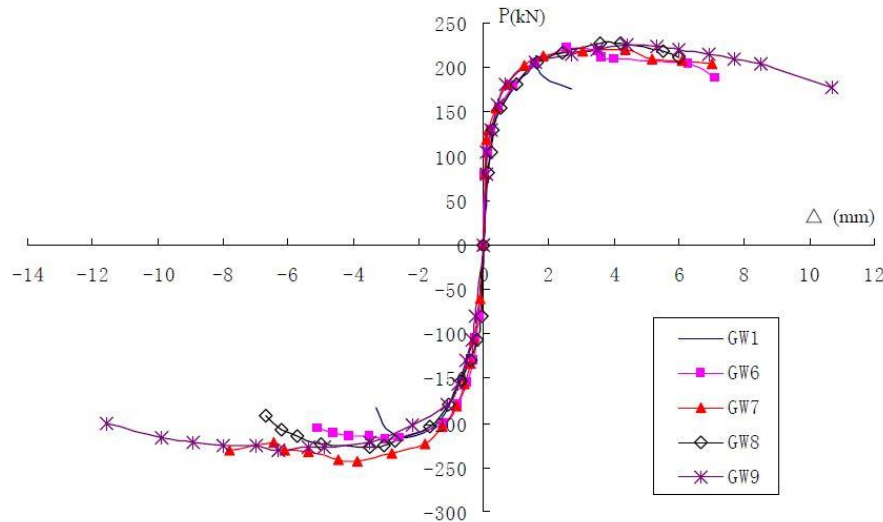


Fig. 7 Continued

Qualitative analysis of seismic performance and the main characteristics of ductility can be analyzed through skeleton curves of lateral load versus deformation (as shown in Fig. 7) by Wang (2003). It can be seen from Fig. 7 that the difference between original stiffness of every specimen was small. This was because of the fact that stiffness of this stage was in relation to the strength of mortar and brick and vertical load. With the increase of horizontal load, the displacement of the bare wall increased better than that of the others and the stiffness began to drop. It also can be seen from Fig. 7 that under the condition of the same displacement, the horizontal load of the bare wall was less than the reinforced specimens, and this tendency was severe with the increase of displacement. Skeleton curve of the bare wall occurred an inflexion at 200 kN, from which a conclusion can be drawn that horizontal load dropped fast after it reached ultimate load and the ultimate displacement less than that of the other specimens.

3.4 Stiffness degradation

With increase of the displacement of structure, the property of loop stiffness of structure becoming small gradually is called stiffness degradation by Zhu (1989). On one hand, secant stiffness of structure under repeated horizontal load can be substituted for tangent stiffness by Wang (2003). On the other hand, according to literature (JGJ101-96), the secant stiffness, which is also named equivalent stiffness, is the ratio of absolute value of summation of repeated horizontal load to summation of the pure displacement in two directions. Stiffness degradation of every specimen was shown in Fig. 8.

It can be seen from Fig. 8 that the curve of stiffness degradation can be divided into three stages: sudden drop stage; calm drop stage and steady stage. Both strengthened specimens and bare specimen (GW1) were of the similar stiffness change due to the fact that the deformations of the specimens were mainly connected to strength of mortar, not the GFRP whose deformations were still little when the horizontal load was relative small. However, with the increase of the pure displacement of the specimens, the stiffness degradation of bare specimen speeded up because of

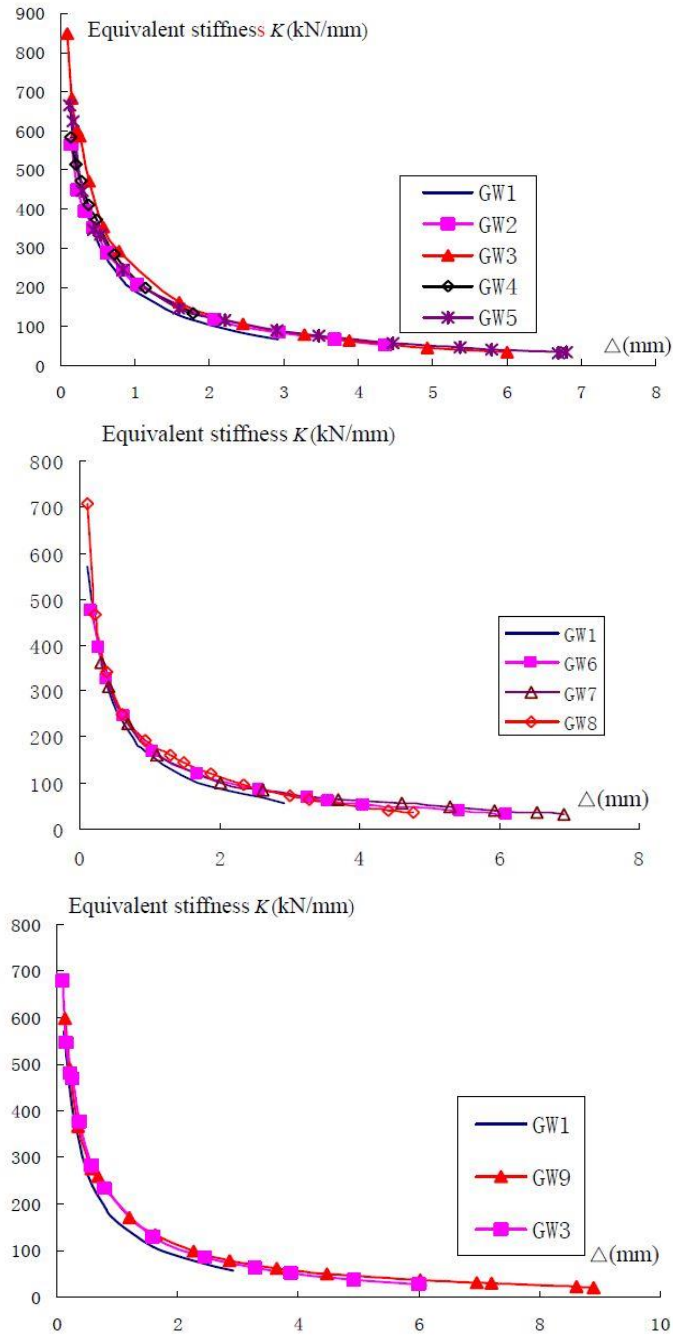


Fig. 8 Stiffness degradation curves

the occurring of the many cracks which was the main factor of leading to lose the load-bearing capacity; on the contrary, the stiffness degradation of reinforced specimens was slowed down with view to the restriction of GFRP.

Table 3 Deformation performance of specimens

Serial number	Loading way	Failure displacement		Failure lateral angle	
		Unidirectional displacement (mm)	Average displacement (mm)	Average lateral displacement ($H=750$ mm)	Increase of displacement (%)
GW1	push	3.22	2.75	1 / 273	0
	pull	2.28			
GW2	push	4.49	4.57	1 / 164	66.0
	pull	4.64			
GW3	push	5.02	5.09	1 / 147	85.1
	pull	5.16			
GW5	push	5.48	5.49	1 / 136	99.6
	pull	5.50			
GW6	push	5.46	6.03	1 / 124	119.2
	pull	6.60			
GW7	push	8.42	7.76	1 / 97	182.3
	pull	7.10			
GW8	push	6.30	6.11	1 / 123	122.0
	pull	5.91			
GW9	push	11.02	9.79	1 / 77	256
	pull	8.56			

Table 4 Influence of reinforcement amount on deformation performance

Area reinforcement ratio (%)	Serial number	Increase of deformation (%)	Average increase (%)
40%	GW2	66.0	93.2
	GW3	85.1	
	GW5	99.6	
	GW8	122.0	
55%	GW6	119.2	185.8
	GW7	182.3	
	GW9	256.0	

3.5 Deformation capacity

Plastic deformation capacity of structure or its components was the expression of ductility property. Ductility of structure which is of the same importance of strength, was the essential criterion of assessing the seismic performance. There were two ways of assessing the seismic performance: the ductility coefficient and relative displacement ductility including cracking lateral angle, ultimate lateral angle and failure lateral angle. Failure lateral angle was used to assess deformation of the specimens in this paper. Deformation capacity of every specimen was shown in Table 3.

3.5.1 Influence of reinforcement amount on deformation

Table 5 Through-wall anchor and related parameter of specimens

FRP type	Width of strips (mm)	Length of strips (mm)	The number of strips	Reinforced specimen with through-wall anchor
GFRP	20	90	16	GW7 、 GW8 、 GW9

Table 6 Influence of anchor on deformation performance

Area reinforcement ratio (%)	Serial number	“Hollow phenomenon”	Anchor measure	Average displacement (mm)	Increase of deformation (%)
40%	GW5	No	No	5.49	11.2
	GW8	Yes	Yes	6.11	
55%	GW6	Yes	No	6.03	28.7
	GW7	Yes	Yes	7.76	

Table 7 Factors and levels of orthogonal analysis

Factor Level	A. Area reinforcement rate (%)	B. Reinforcement mode	C. Anchorage measure
1	40	Gradient	Yes
2	55	Mixed	No

Table 8 Process of orthogonal analysis

Serial Number	Facto Load State	1	2	3	Test results
		A	B	C	Deformation (mm)
GW8		1	1	1	6.11
GW3		1	2	2	5.09
GW6		2	1	2	6.03
GW9		2	2	1	9.79
K_1		11.2	12.1	15.9	The Sum of level index of every factor
K_2		15.8	14.9	11.1	
$k_1=K_1/2$		5.6	6.1	8.0	The Average value of K_1 or K_2
$k_2=K_2/2$		7.9	7.5	5.6	
Relative increase between two levels when factor was same (%)		41.1	23.0	42.9	The Influence of change of test level on deformation perform
Optimum scheme		A_2	B_2	C_1	The optimum specimen (GW9)

It can be seen from Tables 3 and 4 that deformations of the specimens with the surface reinforcement rate of 55 percent was almost twice as much as that of the specimens with the surface reinforcement rate of 40 percent, which showed that the deformation of the specimens can be increased effectively by increasing the reinforcement amount.

3.5.2 Influence of through-wall anchor on deformation

Through-wall anchor and related Parameter of specimens can be seen from Table 5.

It can be inferred from the failure process of specimens and Table 6 that the larger of reinforcement amount, the earlier of occurring of “hollow phenomenon” and the stronger of function of the anchor. Providing that the anchor rate was defined as the ratio of total area of anchors to that of GFRP sheets, the anchor rate of specimen GW8 was 1.4 times as much as GW7,

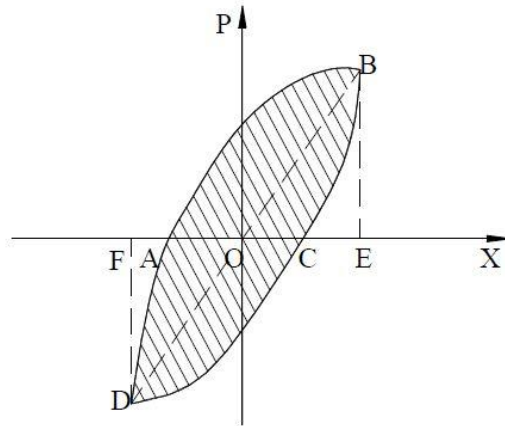


Fig. 9 Calculated sketch map for energy dissipation coefficient (E)

but It can be seen and inferred from Table 6 that the increase of deformation of specimen GW8 was 2.7 times as much as GW7 after being strengthened by through-wall anchor. So it can be concluded from the test results that on the promise of the same anchor amount, the larger the reinforcement of the specimen, the more evident of contribution of anchor to deformation and the more necessary of adopting the through-wall anchor.

3.5.3 Influence of reinforcement mode on deformation

When it came to the influence of reinforcement on the deformation of specimens, orthogonal test method was adopted because of the limited specimens. In this paper, specimen GW3, GW6, GW8 and GW9 can be used to form an orthogonal test with two levels and three factors ($L_4(2^3)$) (as shown in Table 7.), in which the deformation of specimens(failure displacement) were the main indexes to be studied.

It can be inferred through the orthogonal analysis that increasing the reinforcement amount, adopting the mixed reinforcement mode and anchorage measure all contributed to the increase of deformation of the specimens. The influence of reinforcement amount and anchorage measure on deformation had been clarified through the direct contrast, from which the conclusions had been drawn were in accordance with those drawn from the orthogonal test. Moreover, it also can be seen from Tables 7 and 8 that the reinforcement amount and anchor each was almost of the similar effects which was superior to that of the reinforcement mode. Lastly, a fact occurred to us that specimen GW9 was of the best reinforcement mode which had been proved by the test.

3.6 Energy dissipation capacity

The capacity of absorbing energy of structure subjected to low reversed cyclic loading was the reflection of energy dissipation capacity of structure. However, there was the unified criterion of evaluating energy dissipation capacity of structure. At present, the commonly used methods were equivalent viscosity damping coefficient (Wang *et al.* 2003) and energy dissipation coefficient. The later method was adopted in this paper to assess the energy dissipation capacity of specimens at two special states: ultimate load state and ultimate displacement state. The calculated sketch

Table 9 Energy dissipation coefficient (E) of specimens under different load states

Serial number	GW1	GW2	GW3	GW5	GW6	GW7	GW8	GW9
Ultimate load state	1.14	1.05	1.01	0.9	1.07	0.94	0.97	1.09
Ultimate displacement state	1.19	1.21	2.08	1.26	1.31	1.59	1.52	2.42

map for energy dissipation coefficient is shown in Fig. 9. According to literature (China Academy of Building Research, 1997), energy dissipation coefficient (E) can be obtained using Eq. (1) and were shown in Table 9.

$$E = \frac{S_{(ABC+CDA)}}{S_{(OBE+ODF)}} \tag{1}$$

where $S_{(ABC+CDA)}$ =area of the whole hysteresis loop and $S_{(OBE+ODF)}$ =the whole area of ΔOBE and ΔODF .

It can be seen from Table 9 that the value of energy dissipation coefficient (E) in ultimate displacement state was bigger to some degree than that in ultimate load state respectively. On one hand, the value of “ E ” of the bare specimen was bigger than that of the reinforcement specimens in ultimate load state; on the other hand, the energy dissipation capacity of the reinforcement specimens was superior to that of the bare specimen in ultimate displacement state, and the specimens strengthened by mixed mode GFRP were of the better energy dissipation capacity than those strengthened by other modes GFRP.

4. Conclusions

This research has explored the behavior of brick masonry walls with pilaster reinforced by GFRP under in-plane seismic loading. The following conclusions can be drawn from the work.

1. On one hand, GFRP sheets bonded to the wall can be regard as tensile truss rods, the shear strength was effectively increased with the strengthening of the GFRP sheets; on the other hand, the existence of GFRP sheets prevented the propagation of cracks, which improved the seismic performance of the specimens.
2. The deformation of reinforced specimens was mainly influenced by three factors including area reinforcement rate, anchorage measure and reinforcement mode, in which the influence of the last factor on the deformation was less than that of the other two factors which were of the similar influence on the deformation.
3. The ultimate deformation of specimens increased remarkably when was strengthened by GFRP sheets, which was of importance to the collapse of bare masonry buildings.
4. Strengthened by GFRP sheets, the stiffness degradation of the specimens became slower the bare one and the integrity was enhanced after ultimate load; thus, it became little that the probability of sudden collapse of the whole structure due to the brittle failure of the brick masonry walls.
5. Area reinforcement rate, anchorage measure and reinforcement mode had little effect on energy dissipation capacity in the ultimate load state but had much effect in the ultimate displacement state.

6. As far as the energy dissipation capacity in the ultimate displacement state is concerned, the specimens strengthened by mixed mode were superior to that strengthened by horizontal mode or gradient mode.

Acknowledgements

The research reported was financially supported by Hi-Tech Research and Development Program of China (863) under Grant No.2001AA336010. The writers thank the reviewers for their constrictive comments.

References

- Cecchi, A., Milani, G. and Tralli, A. (2004), "In-plane loaded CFRP reinforced masonry walls: mechanical characteristics by homogenization procedures", *J. Compos. Sci. Technol.*, **64**, 2097-2112
- Croci, G.D., Ayala, D.D., Asdia, P. and Palombini, F. (1987), "Analysis on shear walls reinforced with fibre", *IABSE Symp. on Safety and Quality Assurance of Civ. Engrg. Struct., Ind. Assoc. for Bridge and Struct. Engrg.*, Lisbon, Portugal.
- China Academy of Building Research (1997), *Specificating of Testing Methods for Earthquake Resisitance Building (JGJ101-96)*, China Architecture & Building Press, Beijing, China. (in Chinese)
- Ehsani, M.R. (1995), "Strengthening of earthquake-damaged masonry structures with composite material", *Non-Metallic (FRP) Reinforcement for Concrete Structures*, Ed. Taerwe, L., 680-687.
- Ehsani, M.R., Saadatmanesh, H. and Al-Saidy, A. (1997), "Shear behavior of URM retrofitted with FRP overlays", *J. Compos. Constr.*, ASCE, **1**(2), 17-25.
- El-Dakhkhni, W.W., Hamid, A.A. and Elgaaly, M. (2004), "Seismic retrofit of concrete-masonry-infilled steel frames with glass fiber-reinforced polymer laminates", *J. Struct. Eng.*, ASCE, **130**(9), 1343-1352
- ElGawady, M., Hegner, J., Lestuzzi, P. and Badoux, M. (2004), "Static cyclic tests on URM wall before and after retrofitting with composites", *Proceedings of the 13th International Brick and Block Masonry Conference*, Amsterdam.
- ElGawady, M., Lestuzzi, P. and Badoux, M. (2003), "Dynamic in-plane tests on URM", *Response of Structures to Extreme Loadings XL 2003*, Toronto, Canada, August.
- Grande, E., Imbimbo, M. and Sacco, E. (2011), "Simple model for bond behavior of masonry elements strengthened with FRP", *J. Compos. Constr.*, **15**(3), 354-363.
- Hamid, A.A., El-Dakhkhni, W.W., Hakam, Z.H.R. and Elgaaly, M. (2005), "Behavior of composite unreinforced masonry-fiber-reinforced polymer wall assemblages under in-plane loading", *J. Compos. Constr.*, ASCE, **9**(1), 73-83.
- Li, Z.X. (2004), *Theory and Technique of Engineering Structure Experiment*, Press of Tianjin University, Tianjin. (in Chinese)
- Lunn, D.S. and Rizkalla, S.H. (2011), "Strengthening of infill masonry walls with FRP materials", *J. Compos. Constr.*, ASCE, **15**(2), 206-214.
- Moghaddam, H.A. (2004), "Lateral load behavior of masonry infilled steel frames with repair and retrofit", *J. Struct. Eng.*, ASCE, **130**(1), 56-63.
- Rosenboom, O.A. and Kowalsky, M.J. (2004), "Reversed in-plane cyclic behavior of posttensioned clay brick masonry walls", *J. Struct. Eng.*, ASCE, **130**(5), 787-798.
- Prota, A., Manfredi, G. and Nardone, F. (2008), "Assessment of design formulas for in-plane FRP strengthening of masonry walls", *J. Compos. Constr.*, ASCE, **12**(6), 643-649.
- Saadatmanesh, H. (1994), "Fiber composites for new and existing structures", *ACI Struct. J.*, **91**(3), 346-354.
- Schwegler, G. (1994a), "Strengthening of masonry with fiber composites", PhD Thesis, Federal Institute of

- Technology, Zurich, Switzerland. (in German)
- Schwegler, G. (1994b), "Masonry construction strengthened with fiber composites in seismically endangered zones", *Proc. 10th Europ. Conf. on Earthquake Eng.*, The Netherlands, 454-458.
- Sweidan, R.I. (1991), "The application of fiber reinforced plastics to the strengthening of masonry structures", MS Thesis, Dept. of Civ. and Envir. Engrg., Massachusetts Institute of Technology, Cambridge, Mass.
- Stratford, T., Pascale, G., Manfroni, O. and Bonfiglioli, B. (2004), "Shear strengthening masonry panels with sheet glass-fiber reinforced polymer", *J. Compos. Constr.*, ASCE, **8**(5), 434-443.
- Trade Criterion the People's Republic of China (1997), *Specificating of Testing Methods for Earthquake Resistant Building*, (JGJ101-96), Press of Industry of Architecture of China, Beijing. (in Chinese)
- Triantafillou, T.C. (1998), "Strengthening of masonry structures using epoxy-bonded FRP laminates", *J. Compo. Constr.*, **2**(2), 96-104.
- Valluzzi, M.R., Tinazzi, D. and Modena, C. (2002), "Shear behavior of masonry panels strengthened by FRP laminates", *J. Construct. Build. Mater.*, **164**, 09-416
- Wang, L., Wang, T. and Chen, Q. (2003), "Experimental study on performance of concrete-filled rectangular tubular frame under low-reversed cyclic loading", *J. Earthq. Eng. Eng. Vib.*, **23**(3), 115-117. (in Chinese)
- Wang, T. (2003), *Structural Experiment of Civil Engineering*, Press of Wuhan University of Technology, Wuhan. (in Chinese)
- Wang, Y., Ai, J., Zhang, C. and Lu, Z. (2003), "Experimental research on prestressing concrete-masonry wall under low cycle load", *J. Arch. Struct.*, 22-26. (in Chinese)
- Zhu, B. (1989), *Structural Seismic Experiment*, Press of Seismology, Beijing. (in Chinese)